

Challenging the identification of nitride dust in extreme carbon star spectra

K. M. Pitman,¹★ A. K. Speck²★ and A. M. Hofmeister¹★

¹*Department of Earth and Planetary Sciences, Washington University, St. Louis, MO 63130, USA*

²*Department of Physics and Astronomy, University of Missouri-Columbia, Columbia, MO 65211, USA*

Accepted 2006 July 17. Received 2006 June 29; in original form 2006 April 4

ABSTRACT

Nitride dust is predicted to form in small amounts around carbon stars, but the most likely candidate species such as aluminium nitride (AlN) have not yet been detected. Recently, α -Si₃N₄ was inferred to be the main carrier of the 8.5–12.5 μ m absorption band(s) of an extreme carbon star (AFGL 5625), based on comparison with laboratory KBr dispersion spectra. However, this absorption band has also been attributed to silicon carbide (SiC) and C₃. To investigate whether or not nitride dust has truly been detected and if it is present in other extreme carbon stars, we (i) gathered new laboratory infrared (IR) absorbance spectra from a suite of nitride compounds, including Si₃N₄, using the thin film technique which provides correct relative intensities of weak and strong peaks, and (ii) compared these data to *Infrared Space Observatory* Short Wavelength Spectrometer (*ISO* SWS) spectra of seven different extreme carbon stars which also show broad absorption features around \sim 11 μ m. The astronomical data show an apparent continuum of feature shapes ranging from full width at half-maximum (FWHM) of 2 to 2.7 μ m, with peak barycenters ranging from 10.3 to 11 μ m. The previous possible match between the extreme carbon star and Si₃N₄ was also based on many minor peaks longward of the 8.5–12.5 μ m feature. We show that the fit to AFGL 5625 and other extreme carbon stars is unconvincing, because the reported 13–25 μ m features in the observed spectrum are essentially noise. Features due to other nitrides are also not obvious. The apparent continuum of absorption features in the 8.5–12.5 μ m band is better represented by previously published fits of a combination of crystalline (β polytype) and amorphous SiC, where the apparent broadening and shift of the peak barycenter are due to increasing contributions from the amorphous solid.

Key words: methods: laboratory – techniques: spectroscopic – stars: carbon – dust, extinction – infrared: general.

1 INTRODUCTION

Recently, the absorption spectrum of one ‘extreme carbon star’ has been interpreted as arising from silicon nitride (Si₃N₄) dust (Clément et al. 2005). This star type is heavily enshrouded in dust due to recent or ongoing high mass-loss rates; the associated high gas pressures in the dust-forming regions of extreme carbon stars thus provide the potential for forming exotic dust species. To place this object type in the context of stellar evolution, note that stars in the mass range 1–8 M_⊙ eventually evolve up the asymptotic giant branch (AGB) where they begin to lose mass and form circumstellar shells of dust and gas. During their ascent on the AGB, the chemistry of these stars’ atmospheres and circumstellar shells changes as a

result of dredge-up of newly formed carbon from the He-burning shell. Due to the extreme ease of formation and stability of CO molecules, the chemistry in circumstellar shells is controlled by the C/O ratio. If C/O < 1, then all of the carbon is trapped in CO, leaving oxygen to dominate the chemistry. Conversely, if C/O > 1, then all of the oxygen is trapped in CO, and carbon dominates the chemistry. Stars start their lives with cosmic C/O ratios (\approx 0.4), and are thus O-rich. In some AGB stars, the dredge-up of newly formed carbon is efficient enough to raise C/O above unity, and these stars are known as carbon stars (hereafter C-stars). They are expected to have circumstellar shells dominated by amorphous or graphitic carbon grains, although other dust grains are also important [e.g. silicon carbide (SiC)]. Stars with C/O = 1 are known as S-stars and are expected to contain both C- and O-rich dust species, although more exotic nitride and sulphide dust may also be present.

Mass loss is believed to be radiation driven, and, as such, mass-loss rate increases with the increasing stellar luminosity

★E-mail: kpitman@levee.wustl.edu (KMP); speckan@missouri.edu (AKS); hofmeist@levee.wustl.edu (AMH)

associated with the evolution of AGB stars. Thus, the dust shells get thicker (both optically and geometrically), and these stars eventually become invisible at optical wavelengths and very bright in the infrared (IR). Such stars are known as OH-IR stars in the case of O-rich chemistry (Engels et al. 1983), and ‘extreme carbon stars’ for C-rich chemistry (Volk, Kwok & Langill 1992; Volk, Xiong & Kwok 2000). S-stars with such high optical depths have not been observed. In this paper, we will discuss the plausibility of forming and detecting exotic nitride dust species in C-stars and restrict our direct comparison to extreme C-stars.

It is well established that SiC is an important mineral in the dust condensed from C-stars (e.g. Gilra 1971, 1972; Treffers & Cohen 1974; Speck, Barlow & Skinner 1997, and references therein). However, attempts to identify nitride minerals in various dusty astrophysical environments (e.g. novae, planetary nebulae, and late-type binary and C-stars) have thus far proved largely unsuccessful (see summary by Clément et al. 2005 and references therein). Si_3N_4 is of particular interest because this mineral species has been found as pre-solar grains in meteorites (Nittler et al. 1995). Recently, the presence of α - Si_3N_4 has been inferred from the spectrum of a single extreme C-star (AFGL 5625), based upon comparison with KBr pellet dispersion transmission spectra of Si_3N_4 (Clément et al. 2005). If correct, this identification would mark the first detection of silicon nitride (or any nitride) dust in any C-star and in any AGB object. However, meteoritic evidence and theoretical equilibrium calculations disfavour Si_3N_4 as a possible condensate (see Section 2), and comparisons between laboratory absorbances of Si_3N_4 and extreme C-star observations are not necessarily convincing (Section 4). Other nitride compounds more likely to condense as dust have not yet been compared to extreme C-star spectra.

The present paper summarizes theoretical and meteoritic evidence for and against the presence of nitride minerals in the circumstellar envelopes of C-stars (Section 2). We present new laboratory IR thin film absorbance spectra and mass absorption coefficients for several nitride species, including the two major polymorphs of Si_3N_4 (Section 3). Independent confirmation of previous peak positions and strengths for Si_3N_4 is needed because KBr dispersion spectra can have artefacts (cf. Hofmeister et al. 2000b) and because synthesis invariably provides mixtures of the α - and β -polymorphs of Si_3N_4 . In Section 4, we compare our new laboratory measurements to *Infrared Space Observatory* Short Wavelength Spectrometer (ISO SWS; de Graauw et al. 1996; Leech et al. 2003) observations of seven extreme C-stars. Possible spectroscopic matches of nitrides to ISO SWS observations, especially to unidentified astronomical spectral features, are also discussed. We find that dust absorption features in extreme C-stars (e.g. the 8.5–12.5 μm band) cannot be definitively assigned to Si_3N_4 and that recently published fits to SiC and/or C_3 are more probable. A discussion of other possible stellar environments in which nitride dust might form is presented in Section 5.

2 THEORETICAL AND METEORITIC EVIDENCE OF NITRIDE MINERALS AROUND C-STARS

Thermodynamic equilibrium calculations have shown that it is possible for small abundances of some nitride minerals to form in the regions around C-stars, most notably aluminium and titanium nitride (AlN and TiN), whereas the probability of forming Si_3N_4 is

low enough that detection is unlikely (Lodders & Fegley 1995; Lodders & Amari 2005). The pulsation of C-rich AGB and post-AGB stars leads to the generation of moderate shock waves that propagate through the circumstellar shell (Fokin et al. 2001; Schirmacher, Woitke & Sedlmayr 2003). Such shock waves will increase the temperature and density regime in the dust formation zone. Nitrides may be able to form in these shock-enhanced regions. The N abundance in C-stars is assumed to be effectively solar (Lambert et al. 1986; Lodders & Fegley 1997). A recent study found the N abundance in three C-stars to be subsolar to solar (Ohnaka, Tsuji & Aoki 2000). The latter authors suggested that their stars may have formed in a metal-poor region and that the N-abundance was brought up to solar levels by the dredge-up of carbon–nitrogen–oxygen (CNO) products. In their thermochemistry abundance calculations, Lodders & Fegley (1995) varied the N contents of C-stars from 10x to 100x solar values. The minimum N content value was considered to be a high estimate for maximum N content in C-stars (Lambert et al. 1986; Lodders & Fegley 1997). 100x solar N content was considered as an extreme case; such high N contents are probably not possible for these systems, as full C to N conversion excludes C-stars. Even under these elevated N contents, the formation of Si_3N_4 was ruled out. Gas phase SiN has been detected around the best-studied C-stars (IRC+10°216; Turner 1992). However, the abundance is low and the path from gas phase SiN to solid-state Si_3N_4 has not been fully investigated.

Meteoritic evidence does not strongly support the formation of Si_3N_4 around C-stars. The number of Si_3N_4 grains in a meteorite is estimated to be of the order of a few parts per billion (S. Amari, private communication). Based on nitrogen isotopic ratios, the few (~75–100) Si_3N_4 grains studied in meteorites to date can be grouped into three categories. The majority of meteoritic Si_3N_4 grains fall into the solar category ($^{14}\text{N}/^{15}\text{N} \sim 272$; Alexander, Swan & Probro 1994), with comparatively fewer (presumably supernova origin) pre-solar Si_3N_4 grains ($^{14}\text{N}/^{15}\text{N} < \text{solar}$; Nittler et al. 1995; Lin, Amari & Pravdivtseva 2000; Besmehn & Hoppe 2001). Of the ~25 remaining extremely rare pre-solar Si_3N_4 grains discovered in the Indarch (class EH4) meteorite, four Si_3N_4 grains identified via nanoSIMS isotopic analyses had $^{14}\text{N}/^{15}\text{N}$ values $>$ solar and possibly showed a ‘mainstream SiC’ type isotopic trend (cf. Hoppe & Ott 1997) when plotting $^{14}\text{N}/^{15}\text{N}$ versus $^{12}\text{C}/^{13}\text{C}$. For three of these four grains, Amari et al. (2002) were unable to rule out the possibility that the mainstream SiC isotopic signatures observed resulted from small SiC grains attaching to (solar) Si_3N_4 grains. Therefore, to date, only a single grain (Grain ‘A’; Amari et al. 2002) has a definitively intrinsic mainstream SiC isotopic signature. The $^{12}\text{C}/^{13}\text{C} \sim 20$ value reported for Grain A appears to be in the range expected for mainstream SiC ($10 < ^{12}\text{C}/^{13}\text{C} < 100$; Hoppe & Ott 1997), although its carbon isotopes are at the lower limit of the expected range (Amari et al. 2002; S. Amari, private communication). This unique grain is the sole piece of evidence in favour of silicon nitride exhibiting mainstream SiC type properties and therefore occurring as dust around C-stars.

Equilibrium condensation calculations and meteoritic evidence disfavour Si_3N_4 as a dust species, but do not disprove its existence, as conditions in space can differ from those assumed in models, and physical samples constitute but a small fraction of dust proven to exist in space by spectral comparisons. On this basis, we view that it is reasonable to compare laboratory spectra obtained from diverse simple compounds to observational data, but that the validity of such comparisons requires high-quality spectra and careful analysis.

Table 1. Experimental samples: label information and assumed densities.

Mineral name	Purity	Grain size (μm)	Lot number ^a	Comments	ρ_{calc}^b
$\alpha\text{-Si}_3\text{N}_4$	>99.9 per cent metals basis	<1	I25H30	Trace β component	3.170 ^c
$\beta\text{-Si}_3\text{N}_4$	>99.5 per cent metals basis	<44	C31H47	Trace α component	3.170
AlN	? (high)	5–10 nm	n/a	Synthesized (L. Rosen)	3.261
Mg_3N_2	99.6 per cent metals basis	~ 20	G06Q26	–	2.71
Ca_3N_2	99 per cent metals basis	~ 20	I02N38	Packed under 5g Ar	2.608

^aExcept for AlN, all samples were purchased from Alfa/Aesar. High-purity commercial bulk and nanocrystalline forms of AlN have been previously described by Hofmeister, Rosen & Speck (2000a).

^b ρ_{calc} : X-ray crystallography density used in calculating mass absorption coefficient. ρ_{calc} is typically expressed as D_{calc} or D_x in the mineralogical literature. All ρ_{calc} values were obtained for room temperature ($T \sim 20^\circ\text{C}$) samples.

^c ρ_{calc} values for α - and β - Si_3N_4 taken from Yang et al. (1995) and Lide (2005). AlN: National Bureau of Standards (1975), Mg_3N_2 : Lide (2005), cubic Ca_3N_2 : Laurent, Lang & Le Bihan (1968).

3 LABORATORY IR THIN FILM ABSORBANCE SPECTRA

3.1 Experimental samples and techniques

Grain size and manufacturers' information for the powdered nitride samples studied here are presented in Table 1. Our $\alpha\text{-Si}_3\text{N}_4$ sample contains less than 10 per cent $\beta\text{-Si}_3\text{N}_4$ and vice versa; therefore, we performed spectral subtraction [i.e. reduced $I(\nu)$ by $I'(\nu)$ at every ν] via the GRAMS/AITM software package¹ to remove these impurity peaks.

Mineral spectra produced using the thin film method are directly applicable to astrophysical studies without further manipulation of the data (Speck, Hofmeister & Barlow 2000). For each mineral sample, optically thin ($< 1 \mu\text{m}$) films were created via compression in a diamond anvil cell (DAC) sample mount. Each cylindrical component of the DAC (a hollow stainless steel barrel nested about an inner piston) contains a tungsten carbide rocker on to which is mounted a Type II diamond anvil of about 1/3 carat with a culet (or tip) diameter of $\sim 0.6 \text{ mm}$. When the DAC is fully assembled, the two culets are aligned to be concentric, and also parallel by minimizing the interference fringes observed through a binocular microscope. To create a thin film, the bulk sample is first mechanically crushed into nearly micron-sized particulates. The crushed sample is mounded on to one of the diamond tips. Surface tension holds the crushed particulates on to the diamond tip; further compression yields a thin film (thickness $\sim 0.4\text{--}2 \mu\text{m}$) with no visible crosshatching or cracks and little granularity. For each thin film, efforts were made to cover the entire diamond tip with an even layer of sample, but slight irregularities in the thickness were inevitable, partly due to less than perfect alignment of the diamond faces.

Mid- and far-IR absorbance spectra were collected as described by Speck, Hofmeister & Barlow (1999) and Hofmeister, Keppel & Speck (2003). Mid-IR spectra were acquired over the wavenumber range $\sim 4000\text{--}400 \text{ cm}^{-1}$ ($\lambda \sim 2.5\text{--}25 \mu\text{m}$) at 1 or 2 cm^{-1} resolution using a liquid-nitrogen-cooled HgCdTe detector, a KBr beamsplitter and an evacuated Bomem DA 3.02 Fourier transform spectrometer.² The accuracy of the instrument is $\sim 0.01 \text{ cm}^{-1}$. The measured absorbance from the empty DAC serves as the reference spectrum. An Si-bolometer and a coated, broad-band mylar beamsplitter were used for the far-IR range from 50 to 650 cm^{-1} ($\sim 200\text{--}15 \mu\text{m}$) at 1 cm^{-1} resolution. Mid- and far-IR absorbance spectral intensities were scaled to match in the wavenumber region of overlap and

merged. Because scattering increases apparent absorption, the segment with the lowest absorbance values was presumed to be correct.

3.2 Mass absorption coefficient calculations

Many astronomical studies use mass absorption coefficients to estimate the relative abundances and total masses of dust species in a given circumstellar shell (e.g. Albrecht & Chini 2000; Stevens & Gear 2000; Molster et al. 2001; Kemper et al. 2002; Kemper, Vriend & Tielens 2004). We define absorbance and the absorption coefficient in terms of natural logarithms. Let d represent thin film sample thickness, ρ be the density of the thin film, I_{meas} be the measured intensity transmitted through the thin film and I_0 be the intensity incident on the sample. To arrive at the mass absorption coefficient (κ_{abs}), we assume that the transmission coefficient T is

$$T = \exp(-\kappa_{\text{abs}} \rho d), \quad (1)$$

and assume that reflections are accounted for by the reference spectrum, i.e. $T \sim I_{\text{meas}}/I_0$, to obtain

$$\kappa_{\text{abs}} = \ln(I_{\text{meas}}/I_0)/(\rho d). \quad (2)$$

This expression is equivalent to the more familiar

$$\kappa_{\text{abs}}(\lambda) = \tau_{\lambda}/(\rho L), \quad (3)$$

given in Whittet (1992).

Calculated densities (ρ_{calc} ; Table 1) were taken directly from X-ray crystallography (powder diffraction) standards and were checked using the relation

$$\rho_{\text{calc}} (\text{g cm}^{-3}) = (ZM)/(N_{\text{avo}}V), \quad (4)$$

where Z is the number of chemical formula units that each primitive unit cell contains, M is molecular weight, N_{avo} is Avogadro's number and V is cell volume (Klein & Hurlbut 1993). This step was necessary because inconsistent density values were reported by the manufacturer and in the ceramics literature. The meteoritic Si_3N_4 density value (3.11 g cm^{-3} ; Lee et al. 1995) was rejected due to the small size of the crystals for which it was calculated; we instead adopt the density for synthetic nierite for both α - and $\beta\text{-Si}_3\text{N}_4$.

The predominant source of experimental error in κ_{abs} stems from the thin film thickness. From our experience in making thin films, hard materials such as MgO (cf. Hofmeister et al. 2003) tend to produce films in the range $d = 0.8\text{--}1.2 \mu\text{m}$, whereas soft materials such as hydrosilicates (Hofmeister & Bowey 2006) produce films as thin as $d = 0.4 \mu\text{m}$. Of the nitrides studied here, only Ca_3N_2 is soft (deforms easily under pressure) and thus a lower value for d is used in our calculations of κ_{abs} for this material. Other uncertainties in

¹ Thermo Electron Corporation, Waltham, MA.

² Bomem, Inc., Quebec, Canada.

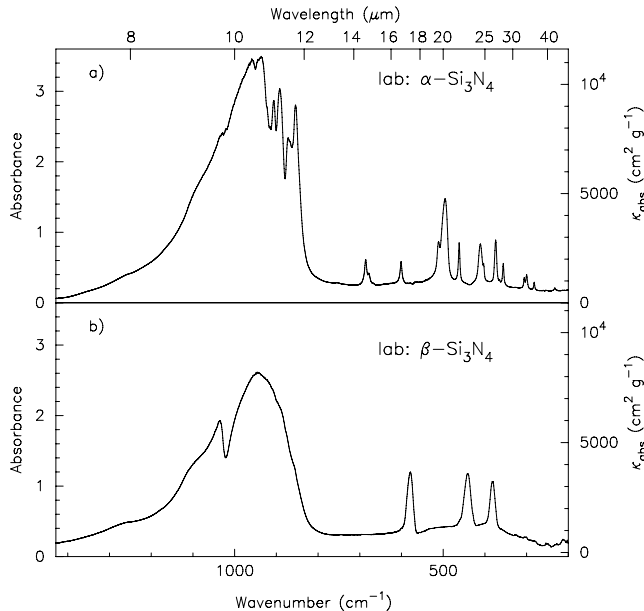


Figure 1. Laboratory natural log absorbance spectra of α - and β - Si_3N_4 . Spectral subtraction to remove trace β - and α - Si_3N_4 components, respectively, has been performed. Significant peaks are located at 10.4, 14.6 and 20.2 μm ; additional peaks are summarized in Table 2.

the measurements (e.g. in absorbance or density, discussed above) are negligible in comparison. As a conservative estimate, we use $d = 0.6 \mu\text{m}$ for Ca_3N_2 and $d = 1.0 \mu\text{m}$ for the remaining nitrides, both with experimental uncertainties of ~ 30 per cent.

3.3 Applicability of laboratory thin film spectra to astronomical environments

3.3.1 Silicon nitride: α , β polytypes

Prominent absorbance peaks in our laboratory IR thin film absorbance spectra of α - and β - Si_3N_4 (Fig. 1) are summarized in Table 2. Peak barycenters were read directly off the spectra, whilst positions for multiple, overlapping peaks were fit with Gaussian–Lorentzian profiles. Our thin film IR absorbance spectra have one peak less than the total number predicted by symmetry analysis for each Si_3N_4 polytype (Tables A1 and A2), as commonly occurs; this peak is probably buried in the envelope of features centred at 1000–900 cm^{-1} (10–11.1 μm).

Our laboratory IR thin film absorbance spectra of α - and β - Si_3N_4 extend to longer wavelengths than the previous KBr dispersion measurements and reveal that α - Si_3N_4 has several additional peaks (Table 2, \star entries). Our β phase has a lower degree of contamination than the β sample measured via KBr dispersion and thus our spectral subtraction should provide more accurate information on its absorption peaks. For α - Si_3N_4 , 14.6 and 20.2 μm features are prominent in the laboratory IR thin film absorbance spectrum; the implications of this finding for extreme C-star spectra are discussed in Section 4.

3.3.2 Aluminium nitride

Among the low abundance elements in C-star circumstellar shells, aluminium has the highest relative concentration. The first aluminium-bearing mineral to form in C-star circumstellar shells is AlN (Lodders & Fegley 1999). As seen in Fig. 2 and as predicted

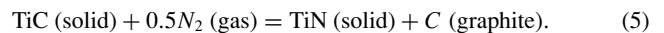
by symmetry analysis (Table A3), two stretching modes result in one main degenerate IR peak at 710 cm^{-1} (14.1 μm), with no other notable absorption features. Bulk and nanocrystalline forms of AlN produce highly similar IR spectra (Hofmeister et al. 2000a). Therefore, if an absorption or emission feature in an astronomical source were to coincide with 14.1 μm , AlN would be among the list of other possible carriers (e.g. C_2H_2).

One question is whether or not AlN would survive long enough to be detected. As the temperature decreases, AlN may quickly transform to corundum (Al_2O_3 ; fig. 6e, Lodders & Fegley 1995). However, in a carbon-rich environment, the low availability of oxygen should preclude transformation of more than a small fraction ($\lesssim 2$ per cent) of the AlN. Only a small fraction (~ 1 per cent) of the dust needs to be corundum to be observable, as argued for O-rich stars (DePew, Speck & Dijkstra 2006). Because no 13- μm features or spectral features of amorphous Al_2O_3 have been found in any C-star spectra (DePew et al. 2006 and references therein), this transformation process is not significant.

Some pre-solar SiC grains contain both TiC and AlN inclusions (Stroud & Bernatowicz 2005). The association of AlN with SiC suggests its formation occurs around C-stars. The relatively low abundances of Al and N in circumstellar shells of C-stars as compared to C or Si may preclude the formation of enough AlN to be detectable in C-star spectra; however, under certain conditions, AlN may be a suitable mineral candidate and its spectral feature should be sought in C-star spectra.

3.3.3 Osbornite (TiN)

The mineral osbornite (TiN) is equally as unlikely as Si_3N_4 to form from the perspective of abundances modelled for C-stars. Lodders & Fegley (1995) discuss the thermochemical reaction of N_2 and TiC to form TiN (equation 5):



For TiN to form, the strong N_2 triple bond must split; although highly unlikely, this reaction may occur $\lesssim 800$ K below the TiC condensation temperature (fig. 4, Lodders & Fegley 1995), producing a low abundance of TiN. As shown in equation (5), a large amount of TiC is required for the formation of TiN. We know that some TiC must form in C-star circumstellar shells because TiC grains have been found inside graphitic pre-solar grains which are believed to originate from C-stars (Bernatowicz et al. 2005; Bernatowicz, Croat & Daulton 2006). However, TiC has not yet been unambiguously identified in C-star spectra (see Li 2003; Speck & Hofmeister 2004), suggesting that only a small amount of TiC is formed. Furthermore, condensation models (Lodders & Fegley 1995; Sharp & Wasserburg 1995) and pre-solar grain evidence (Bernatowicz et al. 2006) suggest that the small TiC grains may become coated in a mantle of carbon, which would preclude the reaction with nitrogen to form TiN. Neither of these arguments strongly supports the formation of detectable amounts of TiN.

Even if TiN were present in small quantities in certain stellar environments (e.g. around high-mass C-stars with high mass-loss rates and relatively high N abundances), it would be virtually impossible to detect. A good laboratory spectrum for TiN absorbance is not available for comparison against astronomical sources, probably due to the electron sharing in the compound’s bonds. In reflectivity measurements, TiN and gold behave similarly; light is highly

Table 2. Mid- and far-IR laboratory absorbance peaks and FWHM of nitrides.

Mineral name	Main peak position ^a		FWHM		Secondary peaks ν (cm ⁻¹) (λ (μ m))
	ν (cm ⁻¹)	λ (μ m)	$\Delta\nu$ (cm ⁻¹)	$\Delta\lambda$ (μ m)	
α -Si ₃ N ₄	961	10.4	244	2.69	~ 1100 (9.091), ^b 1021 (9.794)*, ^c 959 (10.4), 945 (10.6), 935 (10.7), 922 (10.8)*, 915 (10.9)*, 907 (11.0), 891 (11.2), 872 (11.5)*, 867 (11.5), 853 (11.7), ~ 755 (13.2)*, ^d 685.8 (14.58), 678 (14.7), 668 (15.0), 601.2 (16.63), 511 (19.6), 495.3 (20.19), 461.8 (21.65), 411.0 (24.33), 403.0 (24.81), 374.4 (26.71), 365.2 (27.38), 355.8 (28.11), 305.9 (32.69), 300.0 (33.33), 281.8 (35.45), 232 (43.1)*
β -Si ₃ N ₄	944	10.6	233	2.66	1035 (9.662), 942 (10.6), ^e 578.5 (17.29), 441 (22.7), 382.1 (26.17)
AlN	710	14.1	209	4.24	—
Mg ₃ N ₂	547	18.3	301	10.88	3700 (2.703), ~ 446 (22.4), 412.1 (24.27), 350.3 (28.55), 300 (33.3), 232.6 (42.99)
Ca ₃ N ₂	426	23.5	265	16.17	3642 (2.746), ^f ~ 1450 (6.897), ^g 590 (16.9), 425 (23.5), ^e 325 (30.8) ^e

^aThin film absorbance spectra acquired at room temperature are comparable to astronomical spectra (see Section 4.2). Peak positions reported correspond to peak barycenters.

^bItalicized values indicate shoulders. The 1100 cm⁻¹ shoulder is likely to be an longitudinal optic (LO) mode.

^c*Peak not seen in Clément et al. (2005) KBr dispersion spectrum.

^dWeak peak.

^eDoublet.

^fOH peak?

^gMay be 1 or 2 components.

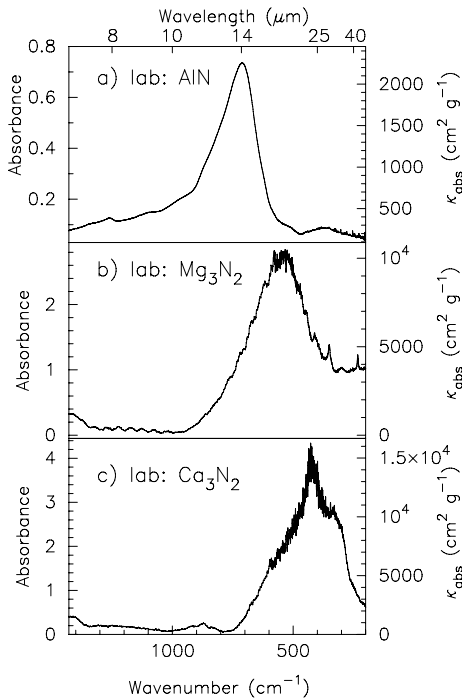


Figure 2. Laboratory natural log absorbance spectra of a suite of nitride thin films: AlN, Mg₃N₂ and Ca₃N₂. The main peaks at 14.1 μ m (AlN), 18.3 μ m (Mg₃N₂) and 23.5 μ m (Ca₃N₂) are due to cation-N stretching modes.

reflected off of the material and does not penetrate the thin film far enough to give a good absorbance spectrum. One strong Ti–N stretching band is expected because this compound is isostructural with cubic NaCl (cf. Wyckoff 1963). Its peak position should be lower in wavenumber than that of the Al–N stretch, given the cation masses. We attempted to acquire a laboratory IR thin film absorbance spectrum of synthetic TiN (99.8 per cent metals basis) and did not detect the expected main peak; the remaining superimposed bands observed were very weak and appeared to be artefacts. Because the main TiN band is too weak to be measured in the laboratory, we can therefore reasonably expect to rule out the detection of TiN via astronomical observations.

3.3.4 Magnesium and calcium nitrides [(Mg, Ca)₃N₂]

In addition to the above nitrides, which have all been considered as possible condensates in astrophysical environments, we also measured laboratory IR thin film absorbance spectra for magnesium nitride (Mg₃N₂) and calcium nitride (Ca₃N₂), both of which have known strong absorbance features that may also be seen in extreme C-star spectra (see Section 4) at around 30 μ m and lesser features in the 15 μ m range (cf. Nyquist & Kegel 1971). The nucleosynthesis in C-stars does not significantly affect Mg or Ca, so cosmic relative abundances apply for these elements. Mg is roughly as abundant as Si and Fe; Ca is a little less abundant than Al but significantly more abundant than Ti. Ca-bearing dust species have been seen around O-rich AGB stars (Demyk et al. 2000), indicating that Ca could potentially form in observable quantities of dust around C-rich AGB stars as well. The inclusion of Ca in dust formation in reducing environments has not been well investigated. Aside from nitrides, sulphides are also expected to be the carriers of Mg and Ca [see

Hofmeister et al. (2003) and Begemann et al. (1994) for sulphide laboratory spectra].

Because these substances deteriorate in air (i.e. surface hydration creates additional peaks not associated with the bulk compound), multiple runs were acquired to determine which peaks were intrinsic. The best and most consistent thin film absorbance spectra are shown in Fig. 2; spectral peak locations for these nitrides are in Table 2. The only bands of interest to astronomers are the main peaks, located at 18.3 and 23.5 μm for Mg_3N_2 and Ca_3N_2 , respectively.

From symmetry analyses (Table A4), 16 IR peaks are predicted for $(\text{Mg}, \text{Ca})_3\text{N}_2$; we found six of these peaks in our spectra. Only the position of the main peak can be taken as definite; this is due to Mg-N or Ca-N stretching. The lower frequency of the main cation-N stretching peak in Ca_3N_2 as compared to Mg_3N_2 is caused by the larger mass of Ca^{2+} and is consistent with a simple harmonic oscillator model (i.e. $\nu = \sqrt{k/m}$, where k is force constant and m is reduced mass). Because Al^{3+} has a higher charge than Mg^{2+} and thus creates a stronger force constant, AlN has a higher frequency IR band than Mg_3N_2 , even though the cation masses are the same. Similarly, the $\text{Si}^{4+}\text{-N}$ stretch has a higher ν than $\text{Al}^{3+}\text{-N}$ (cf. Batsanov & Derbeneva 1969). Unlike the main stretching peaks in the other nitride species, the $\text{Ca}^{2+}\text{-N}$ peak is a resolved doublet. Weak peaks for both $(\text{Mg}, \text{Ca})_3\text{N}_2$ are likely to be present at low wavenumbers.

3.4 Comparison of thin film and KBr spectra

Clément et al. (2005) noted that their KBr pellet dispersion transmission spectra do not reproduce previous IR laboratory measurements of silicon nitrides obtained from vapour-deposited thin films (e.g. Yin & Smith 1990; Klanjšek Gunde & Maček 2001), calling into question the differences between the laboratory methodologies. Instead, the differences between the (vapour-deposited) thin film and the KBr dispersion IR spectra are clearly due to the variety of chemical compositions examined, and accompanying variations in structure, rather than to laboratory techniques. Yin & Smith (1990) studied amorphous, hydrogenated silicon nitrides, with varying ratios of H, Si and N. Similarly, Klanjšek Gunde & Maček (2001) examined oxygenated silicon nitride, in which O, Si and N are present in unknown proportions. The amorphous sample of Clément et al. (2005) was not purposefully hydrogenated and therefore should not have the same IR spectra of the previous H- and O-rich amorphous samples.

We found good agreement in peak positions and in relative intensities overall between IR spectra gathered from powder dispersed in KBr and from our (particulate) thin films of crystalline Si_3N_4 with fixed stoichiometry and structure (Fig. 1). Our films are typically 0.3–1.5 or 2 μm thick. Particle sizes used in the KBr method are typically below $\sim 0.3 \mu\text{m}$. Even dispersion of mineral powder in the

KBr pellet should therefore produce absorbance spectra compatible with those obtained from thin films.

4 ASTRONOMICAL SOURCES

Clément et al. (2005) suggested that a broad, double-peaked 8.5–12.5 μm absorption feature in the *ISO* SWS spectra of AFGL 5625 and possibly AFGL 2477 is due to the α -polytype of silicon nitride. This identification was also based on matching several weak absorption features in the 13–35 μm region. However, their analysis shows that only AFGL 5625 looks like a promising match and that alternate carriers of the 8.5–12.5 μm feature cannot be excluded for AFGL 2477; other C-stars with similar features were not analysed.

Using our results for α - and β - Si_3N_4 , we now reinvestigate the possibility that silicon nitride dust has been detected by comparing our laboratory data to a larger set of extreme C-stars, including a more recently discovered extreme C-star with a similar broad 8.5–12.5 μm feature. We also discuss briefly the appearance in extreme C-star spectra (or lack thereof) of features associated with other nitrides.

At the high optical depths found in the circumstellar shells of extreme C-stars, the classic 11- μm emission feature is no longer seen. Speck, Thompson & Hofmeister (2005) showed that seven of the extreme C-stars in that study exhibited several absorption features in the 8.5–12.5 μm range. In AFGL 3068 and IRAS 02408+5458, two of those absorption features have been definitively attributed to β -SiC (Speck et al. 1997; Clément et al. 2003). Two additional absorption features in the 8.5–12.5 μm range, found in the spectra of AFGL 2477 and AFGL 5625, have been attributed to Si_3N_4 (Clément et al. 2005), to amorphous SiC (Speck et al. 2005) and also to a combination of circumstellar β -SiC and interstellar silicate (Speck et al. 1997). We have obtained and analysed *ISO* SWS spectra of all seven extreme C-stars which exhibit absorption features in the 8.5–12.5 μm range.

The astronomical spectra were observed using the *ISO* SWS (de Graauw et al. 1996) and reduced via pipeline version OLP10.1 from the *ISO* data archive. Individual spectral sub-bands were cleaned from glitches (caused by cosmic ray particles) and other bad data sections. Results were then flat-fielded and sigma-clipped. The final resolution varies from $\lambda/\Delta\lambda = 200$ to 400. Table 3 summarizes the extreme C-stars observed, whereas Fig. 4 shows both their 5–45 μm flux-calibrated and 5–25 μm continuum-divided spectra.

4.1 Continuum-fitting the spectra

The emission at wavelength λ from a dusty region with optical depth $\tau(\lambda)$ and a single temperature T is

Table 3. Extreme C-stars analysed for Si_3N_4 .

Source	IRAS name	RA (J2000) ^a	Dec. (J2000)	TDT number	Date of observation	T_{cont}	β
	IRAS 00210+6221	00 23 51.196	+62 38 16.4	40401901	1996 Dec 24	250	1
	IRAS 02408+5458	02 44 25.2	+55 11 15	80002504	1998 Jan 24	250	0
	IRAS 06582+1507	07 01 08.44	+15 03 39.8	71002102	1997 Oct 26	320	0
AFGL 5416	IRAS 17534–3030	17 56 33.09	–30 30 47.1	12102004	1996 Mar 17	235	1
AFGL 2477	IRAS 19548+3035	21 50 45.00	+53 15 28.0	56100849	1997 May 30	295	0
AFGL 5625	IRAS 21318+5831	21 33 22.98	+56 44 35.0	11101103	1997 Mar 7	245	1
AFGL 3068	IRAS 23166+1655	23 19 12.39	+17 11 35.4	37900867	1996 Nov 29	290	0

^aNote: units of right ascension are given in hours, minutes and seconds; units of declination are degrees, arcmin and arcsec. *ISO* observation mode: SWS01. T_{cont} : continuum temperature, given in K.

$$F(\lambda) \propto B(\lambda, T) \{1 - e^{-\tau(\lambda)}\}, \quad (6)$$

where $B(\lambda, T)$ is the Planck function.

When the source is optically thick, $F(\lambda) \propto B(\lambda, T)$; otherwise $F(\lambda) \propto B(\lambda, T) \times \kappa(\lambda)$, where $\kappa(\lambda)$ is the grains' wavelength-dependent absorption coefficient. The source will emit as a blackbody when either $\tau(\lambda) \gg 1$ or $\kappa(\lambda)$ is wavelength independent (grey opacity). At low optical depths, the absorption coefficient is $\kappa(\lambda) \propto \lambda^{-\beta}$ so that

$$F(\lambda) \propto B(\lambda, T) \times \lambda^{-\beta}. \quad (7)$$

The index β depends on the size, structure and composition of the grains. Grains with an amorphous structure tend to have β close to unity; for crystalline dust grains, β tends to be closer to 2. We can therefore use the index β to determine some aspects of the nature of the emitting dust grains.

With this in mind, we fitted a continuum to the 2–45 μm spectrum. Where available, we used the model spectral energy distributions (SEDs; AFGL 5416, IRAS 00210+6221 and IRAS 06582+1507) from Volk et al. (2000); otherwise we used either a blackbody or a blackbody times an emissivity ($\lambda^{-\beta}$) and iterated on combinations of T and β to provide the best fits, allowing for known features (e.g. the '30 μm ' MgS emission feature; C_2H_2 absorptions). Although radiative transfer (RT) models are the preferred continua, very similar continua are achieved by the simpler blackbody fitting (Speck et al. 1997; Clément et al. 2003, 2005). Continuum-divided spectra produced by division by either a model SED or a blackbody are essentially identical, with the only major difference between the model continua and the (modified) blackbody continua occurring in the region of the '30- μm ' feature. This is illustrated in Fig. 3. The resulting best fits to the continua are shown in Fig. 4, and the continuum temperatures are listed in Table 3. The blackbody fits are near room temperature, suggesting that peak shifts in laboratory spectra due to heating and/or cooling are unimportant (i.e. that our room temperature laboratory spectra are appropriate for comparison). That the majority of our observed spectra are best fit with a pure blackbody implies that the dust is optically thick at IR wavelengths and that we are seeing a surface in the dust shell at the continuum temperature.

AFGL 3068 is the prototype for the extreme C-star class (Jones et al. 1978; Speck et al. 1997); its continuum-divided spectrum closely resembles that of IRAS 02408+5458. In particular, both objects exhibit an absorption feature peaking at $\sim 11 \mu\text{m}$ with full width at half-maximum (FWHM) of $\sim 2 \mu\text{m}$. This is narrower than the 8.5–12.5 μm features in the remaining objects. Both AFGL 2477 and 5625 have much broader absorption with barycenters at $\sim 10.3 \mu\text{m}$ and FWHM of $\gtrsim 2.5 \mu\text{m}$. These broad features resemble that of IRAS 00210+6221 in shape, strength and position. IRAS 06582+1507 and AFGL 5416 have 8.5–12.5 μm absorption features that appear to be intermediate between the broad and narrow extremes. The rise in the slope of the continuum-divided spectra at wavelengths $> 20 \mu\text{m}$ is due to the onset of the '30- μm ' feature (e.g. Volk et al. 2000). Because we see an apparent continuum of 8.5–12.5 μm feature widths ranging from narrow (AFGL 3068) to broad (AFGL 5625), it is possible that the carriers responsible for these features are related. If this is the case and if a single carrier is responsible, then this supports the previous attribution of this feature to SiC; the narrow features in the extreme C-star *ISO* spectra would then be due to crystalline (β -) SiC, while progressively more amorphous SiC contributions would lead to the broadening. Alternatively, the progression from narrow to broad could be an increasing contribution from C_3 in addition to crystalline SiC (Zijlstra et al. 2006), which would broaden the SiC absorption feature to the blue

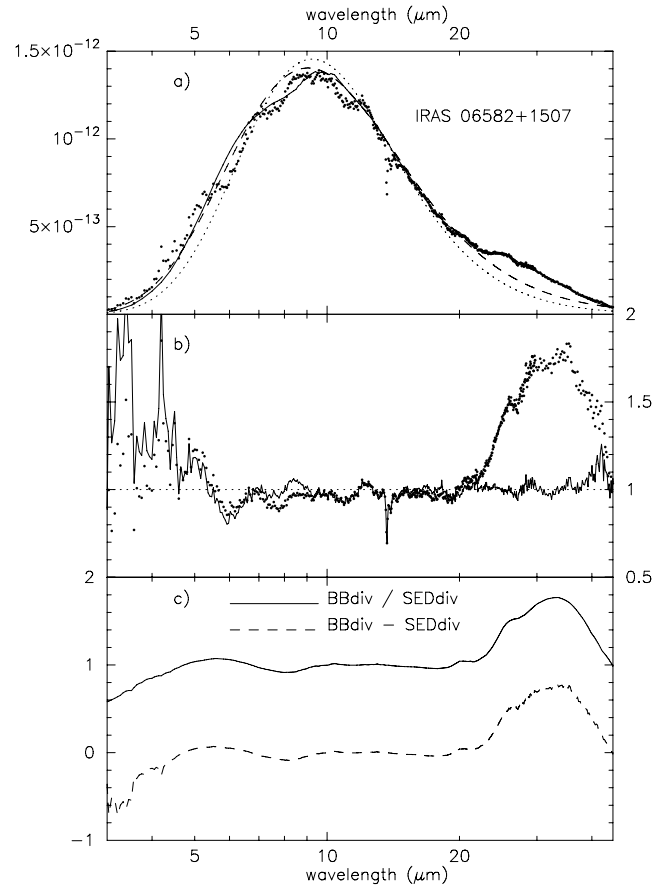


Figure 3. Comparison of continuum fits. Upper panel: the flux-calibrated *ISO* SWS spectrum (round points) of the extreme C-star IRAS 06582+1507 together with the best-fitting blackbody continuum (dashed line), blackbody $\times \lambda^{-1}$ (dotted line) and the RT model SED fit from Volk et al. (2000) (solid line). The y-axis is the log flux (F_λ) in $\text{W m}^{-2} \mu\text{m}^{-1}$; the x-axis is wavelength in μm . Optical constants for amorphous carbon (Rouleau & Martin 1991) were used in the RT model; Gaussian absorptions included by Volk et al. (2000) to match observed molecular features cause the slight dip between 7 and 9 μm (solid line). Centre panel: the *ISO* SWS spectrum of IRAS 06582+1507 is given, divided by the simple blackbody (points) and divided by the Volk et al. (2000) RT model SED (solid line). Lower panel: comparison of the continuum-divided spectra. The solid line represents the blackbody-divided spectrum divided by SED-divided spectrum. The dashed line represents the difference between the blackbody-divided spectrum and the SED-divided spectrum. These comparisons demonstrate the validity of using a blackbody continuum for analysing spectral features (see Section 4.1), especially in the 8.5–12.5 μm region. The y-axis is dimensionless; the x-axis is wavelength in units of μm .

side. The transition from SiC for the narrow features to Si_3N_4 for the broad features seems less likely on the grounds that the physical nature of the shells in these objects is not sufficiently different to account for that large of a change in chemistry. Comparing the model parameters from table 3, Volk et al. (2000; e.g. mass-loss rate, optical depth, brightnesses, density distribution, chemistry) of four of the extreme C-stars in Fig. 4, the dust shells are broadly similar in all parameters. Upon closer examination of the model parameters, one can identify two pairs of models for which the parameters are almost identical. However, these pairings do not correlate with the breadth of the 11 μm absorption feature. The attribution of the blue side of the broad feature to C_3 is a little troublesome in that this feature should be accompanied by a stronger absorption at $\sim 5 \mu\text{m}$. This

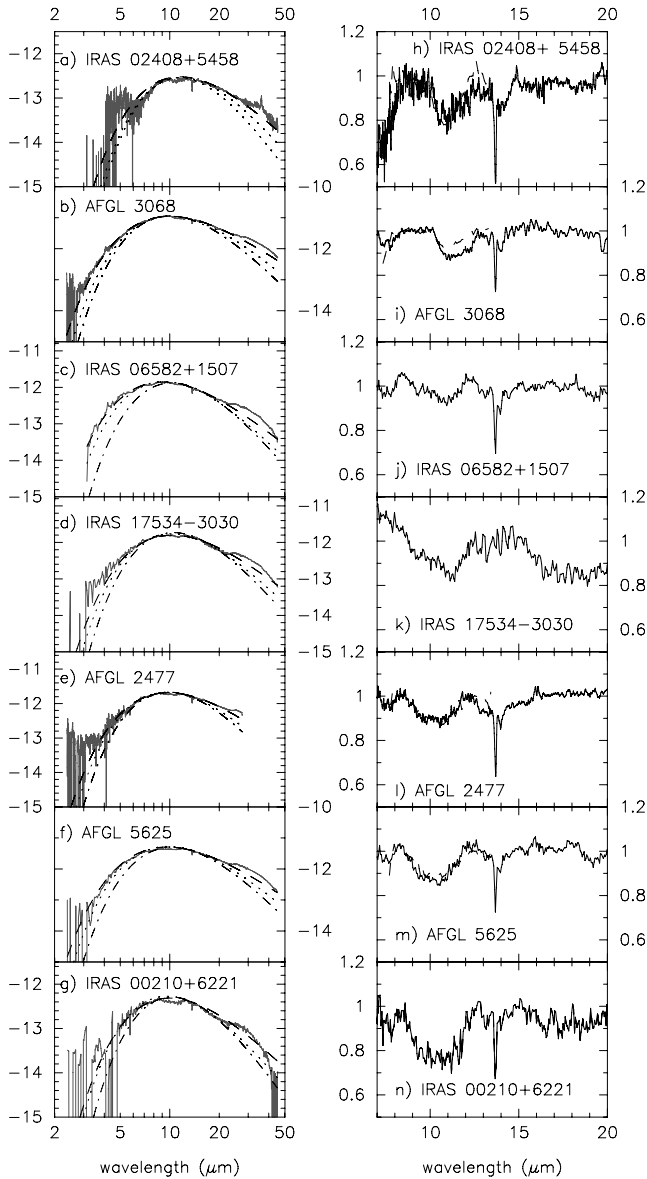


Figure 4. *ISO* SWS spectra of seven extreme C-stars. Left-hand panel: flux-calibrated spectra and fitted continua. Grey line = *ISO* spectrum; dashed line = best-fitting blackbody continuum; dotted line = best-fitting modified blackbody continuum with $\beta = 1$; dot-dashed line = best-fitting modified blackbody continuum with $\beta = 2$. The y-axis is the log flux (F_λ) in $\text{W m}^{-2} \mu\text{m}^{-1}$; the x-axis is wavelength in μm . Right-hand panel: continuum-divided spectra. Solid line = *ISO* spectra; dashed line = ground-based spectra from Speck et al. (1997). Table 3 lists the continua used in each case to produce the continuum-divided spectra.

absorption is not seen in any of the *ISO* objects listed in Table 3. We therefore favour the attribution of this feature wholly to SiC with the variation in breadth/barycenter caused by changes from crystalline to amorphous SiC (Speck et al. 2005).

4.2 *ISO* continuum-divided spectra: identifying peaks versus noise

Starting with the original flux-calibrated *ISO* data, we noted points in the spectra which might give rise to spectral dips or shifts in the continuum position and exclude those wavelengths from our peak

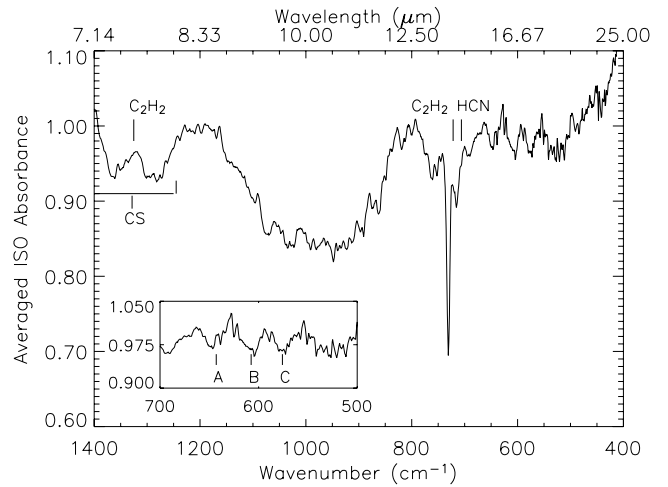


Figure 5. Average of the continuum-divided spectra of three *ISO* extreme C-stars: IRAS 00210+6221, AFGL 5625 and AFGL 2477. Theoretical positions of molecular bands from Aoki, Tsuji & Ohnaka (1999) are marked: CS = 7–8 μm , $\text{C}_2\text{H}_2(\nu_4 + \nu_5) = 7.5 \mu\text{m}$, $\text{C}_2\text{H}_2(\nu_5) = 13.7 \mu\text{m}$ and $\text{HCN}(\nu_2) \sim 14 \mu\text{m}$. Letters A, B and C denote plausible weak absorption features in the spectrum located at $\lambda \sim 15.5$, 16.4 and 17.3 μm , respectively. The FWHM of feature A is $\sim 0.25 \mu\text{m}$; features B and C have FWHM values of $\sim 0.5 \mu\text{m}$.

assignments. Those processing artefacts may occur at 12, 16.3 and 19.4 μm where the individual *ISO* subspectra are spliced together.

Distinguishing true features from the noise threshold of *ISO* continuum-divided spectra is also a primary concern. To eliminate noise and to determine what features are likely to be present in an extreme C-star, we have averaged the continuum-divided spectra of three stars (IRAS 00210+6221, AFGL 5625 and AFGL 2477) to create a simple template of the behaviour from ~ 7 to 25 μm (Fig. 5). We selected these three spectra for the average because they have the most similar 8.5–12.5 μm features in terms of shape and position. AFGL 3068 and IRAS 02408+5458 were purposely excluded from the average because Clément et al. (2003, 2005) attribute the spectral features in those objects to β -SiC rather than Si_3N_4 .

In Fig. 5, the dominant feature is a broad absorption band located between wavelengths ~ 8.5 and 12.5 μm . Three weaker yet plausible absorption features occur in the 15–20 μm wavelength range, appearing at ~ 15.5 , 16.4 and 17.3 μm . The 16.4- and 17.3- μm features appear to have an off-centred peak (dip). The 16.4- μm feature is close to the 16.3 μm artefact of splicing subspectra. The remaining features at 15.5 and 17.3 μm are not located close to splice points and could be potentially intrinsic to extreme C-star spectra in general. We consider the possibilities that these features are due to instrumental effects, due to observational assumptions or due to an actual carrier. The weak 15.5- μm feature is most suspect. Comparing the averaged C-star spectrum to the individual *ISO* spectra, we do not see the 15.5- μm feature; therefore, this feature may be due to noise. We have verified that the weak feature at 15.5 μm was not present in the calibrator. Considering the possibility that real carriers are responsible for the 15.5 and 17.3 μm features, the narrowness of these features may imply atomic or molecular origin. There is a strong interstellar [Ne III] line at 15.5 μm , and polycyclic aromatic hydrocarbon (PAH) emission features have been previously identified at both 15.5 and 17.3 μm , although such features are not typically seen in absorption (e.g. Bregman & Temi 2001). Therefore, only the weak 17.3- μm feature may be possibly intrinsic to extreme C-star spectra. Clearly, the spectra in Figs 4 and 5 do not show any

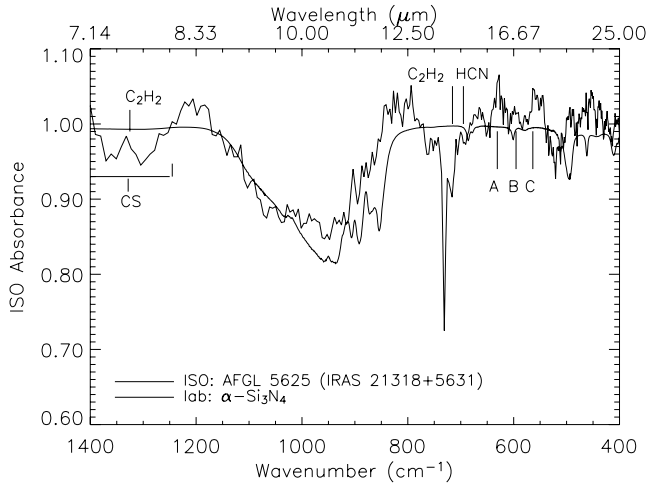


Figure 6. *ISO* SWS continuum-divided spectrum of AFGL 5625 (solid line), compared to the laboratory IR thin film absorbance spectrum of α - Si_3N_4 (dashed line). The natural log absorbance of α - Si_3N_4 was multiplied by a scaling factor of 0.0525, then subtracted from 1.0 to generate this overlay. Features not shown at $\lambda > 25 \mu\text{m}$ are essentially noise (see fig. 5, Clément et al. 2005).

obvious spectral features that could be associated with the other nitrides presented in Section 3.3 (AlN , $[\text{Mg,Ca}]_3\text{N}_2$). Consequently, we do not perform an in-depth analysis to try to match these features.

Purely on the basis of spectral matching, the silicon nitride laboratory absorbance spectral features and *ISO* continuum-divided spectra presented in Clément et al. (2005) do not coincide in the 13–25 μm region. A comparison between the laboratory absorbance spectrum of α - Si_3N_4 and the *ISO* SWS spectrum of AFGL 5625 clearly shows the mismatch in peak profiles (Fig. 6). For the case of AFGL 5625, the scaled laboratory α - Si_3N_4 spectrum has more intensity on the red side of the main 8.5–12.5 μm feature; the laboratory spectral features are shifted in wavelength position relative to the *ISO* SWS spectrum at $\sim 11 \mu\text{m}$ and also at ~ 19 and $21 \mu\text{m}$ (fig. 5, Clément et al. 2005). We estimated the signal-to-noise ratio (S/N) by inspection, noting the absolute displacement of the continuum (noise in flux units) and measuring the depth of absorption (signal). Ideally, a *bona fide* mineral detection is made at the 3σ level; a ‘feature’ detection at less than 2σ is in fact noise. The S/N for the main broad 8.5–12.5 μm feature is $S/N \sim 6$. In their laboratory absorbance spectrum of Si_3N_4 (fig. 5, Clément et al. 2005), the depth of the 20.2 μm absorption feature appears to be greater than 50 per cent of the depth of the main 8.5–12.5 μm feature. Assuming that the 20.2- μm feature is half as deep as the 8.5–12.5 μm feature, this implies that the 20.2- μm feature should be detectable in the spectrum of AFGL 5625 with a S/N of ~ 4 . The weak ‘features’ noted by Clément et al. (2005) all have $S/N < 2$ and therefore cannot be considered true matches. In the remaining *ISO* extreme C-star spectra, the dip centred at $\sim 19.2 \mu\text{m}$ with a S/N of 2.66 is the most plausible absorption feature; however, it occurs 0.4 μm shortward of where the closest laboratory Si_3N_4 absorbance feature should fall.

5 CONCLUSIONS

We have presented new laboratory IR absorbance spectra and mass absorption coefficients of several nitride species which may be relevant to astrophysical environments. Based on interstellar abundances for C-stars, we conclude that Si_3N_4 is unlikely to form in

those systems and is therefore not a dominant dust species. We have investigated the likelihood of forming and detecting alternate nitrides. AlN is more likely than Si_3N_4 to form in C-stars; Mg_3N_2 and Ca_3N_2 are equally as (un)likely to form as Si_3N_4 . TiN has little chance of being detected; none of the remaining nitride species can be successfully matched to the *ISO* extreme C-star spectra studied here.

Whilst the theoretical models argue against the formation of Si_3N_4 around C-stars (and, by analogy, extreme C-stars), model predictions must be tested by spectral comparisons before the formation of the compound in these environments can be definitively ruled out. Nitride dust has been tentatively identified in the *ISO* continuum-divided spectrum of one extreme C-star (AFGL 5625), based upon laboratory mid- and far-IR spectra of crystalline Si_3N_4 (Clément et al. 2005). Although our independently produced laboratory absorbance spectra of α - and β -polytype Si_3N_4 (particulate) thin films appear to be in agreement with those authors’ KBr pellet laboratory results, the spectral signature of silicon nitride is an unconvincing match to AFGL 5625. The silicon nitride laboratory absorbance spectral features are shifted in wavelength position relative to the presumed corresponding *ISO* continuum-divided spectral features; several of the astronomical continuum-divided spectral features presented in Clément et al. (2005) cannot be considered true features given the S/N involved. Previous attribution of the observed broad 8.5–12.5 μm feature to either SiC transforming from crystalline to amorphous, or crystalline (β -) SiC together with the molecule C_3 , are more plausible candidates for this feature. On this basis, no definitive identification of nitride dust around extreme C-stars (or any AGB-type object) has yet been made.

The fact that nitride dust has not yet been detected around extreme C-stars and seems unlikely to form and/or be detected around the larger class of C-stars does not preclude its existence in other stellar environments. Considering the case of O-rich stars, AlN is not generally expected in O-rich environments but could be considered a candidate for O-rich objects in which an unidentified 14- μm feature is seen but not a 13- μm feature, e.g. HV 2310 (Sloan et al. 2006). However, non-spherical corundum or spinel grains also exhibit a spectral feature at $\sim 14 \mu\text{m}$ (see DePew et al. 2006), and are, thus, possibly more plausible dust products in such a system. The main difficulty in conclusively detecting AlN in O-rich stars would be isolating the main AlN peak from the spectral signatures of these competing carriers. Mg_3N_2 is not expected to occur around O-rich stars, because the Mg is likely to be tied up in silicates (and spinel). Ca-rich species are present in dust around O-rich stars, but Ca-rich condensates are rarely considered for O-rich stars. SiN/HNSi molecular gas is expected to form in C-star environments (MacKay & Charnley 1999). Indeed, gaseous SiN molecules have been detected in the spectrum of well-studied C-stars, IRC+10°216 (Turner 1992). In S-stars, the majority of C and O atoms tend to be trapped in CO molecules, thus allowing different elements to be incorporated into dust grains. Whereas FeSi has been predicted to dominate the dust in S-stars (Ferrarotti et al. 2000; Ferrarotti & Gail 2002), SiN/HNSi , solid-state AlN , molecular TiN and molecular (Mg, Ca) $_3\text{N}_2$ have not yet been included in models of S-star dust. Therefore, the circumstellar regions of S-stars may be the most promising place to find observable quantities of AGB nitride dust, and will be the subject of a future paper.

ACKNOWLEDGMENTS

This work was supported by NASA APRA04-000-0041. The authors thank E. Keppel for her help in obtaining the laboratory IR

spectra and G. Thompson (University of Missouri-Columbia) for his assistance with the *ISO* data reduction. The authors also thank K. Lodders and S. Amari (Washington University, St. Louis) for helpful discussions on interstellar abundances, K. Volk (Gemini) for providing us with his model fits for extreme C-stars and anonymous reviewers for careful comments on improving the presentation of this paper.

REFERENCES

- Albrecht M., Chini R., 2000, Meeting Abstract. Instituto de Radioastronomía Millimétrica (URAM), Universidad de Granada and Instituto de Astrofísica de Andalucía (IAA)
- Alexander C. M. O'd., Swan P., Probro C. A., 1994, *Meteoritics*, 29, 79
- Amari S., Jennings C., Nguyen A., Stadermann F. J., Zinner E., Lewis R. S., 2002, *Lunar Planet. Sci. Conf.*, 33, 1205
- Aoki W., Tsuji T., Ohnaka K., 1999, *A&A*, 350, 945
- Batsanov S. S., Derbeneva S. S., 1969, *J. Struct. Chem.*, 10, 510
- Begemann B., Dorschner J., Henning T., Mutschke H., Thamm E., 1994, *ApJ*, 423, L71
- Bernatowicz Th. J., Akande O. W., Croat Th. K., Cowsik R., 2005, *ApJ*, 631, 988
- Bernatowicz Th. J., Croat Th. K., Daulton T. L., 2006, in Lauretta D. S., McSween H. Y., eds, *Meteorites and the Early Solar System II*. Univ. Arizona Press, Tucson, AZ, p. 942
- Besmehn A., Hoppe P., 2001, *Lunar Planet. Sci. Conf.*, 32, 1188
- Bregman J. D., Temi P., 2001, *ApJ*, 554, 126
- Clément D., Mutschke H., Klein R., Henning Th., 2003, *ApJ*, 594, 642
- Clément D., Mutschke H., Klein R., Jäger C., Dorschner J., Sturm E., Henning Th., 2005, *ApJ*, 621, 985
- de Graauw Th. et al., 1996, *A&A*, 315, L49
- Demyk K., Dartois E., Wiesemeyer H., Jones A., D'Hendecourt L., Jourdain de Muizon M., Heras A. M., 2000, in Salama A., Kessler M. F., Leech K., Schulz B., eds, *ESA-SP 456, ISO Beyond the Peaks: The 2nd ISO Workshop on Analytical Spectroscopy*. ESA Publications Division, Noordwijk, p. 183
- DePew K., Speck A., Dijkstra C., 2006, *ApJ*, 640, 971
- Engels D., Kreysa E., Schultz G. V., Sherwood W. A., 1983, *A&A*, 124, 123
- Fateley W. G., McDevitt N. T., Bentley F. F., 1971, *Appl. Spectrosc.*, 25, 155
- Ferrarotti A. S., Gail H.-P., 2002, *A&A*, 382, 256
- Fokin A. B., Lèbre A., Le Coroller H., Gillet D., 2001, *A&A*, 378, 546
- Gilra D. P., 1971, *Nat*, 229, 237
- Gilra D. P., 1972, PhD thesis, Univ. Wisconsin, Madison
- Hofmeister A. M., Bowey J. E., 2006, *MNRAS*, 367, 577
- Hofmeister A. M., Rosen L. J., Speck A. K., 2000a, in Sitko M.L., Sprague A.L., Lynch D.K., eds., *ASP Conf. Ser. Vol. 196, Thermal Emission Spectroscopy and Analysis of Dust, Discs, and Regoliths*. Astron. Soc. Pac., San Francisco, p. 291
- Hofmeister A. M., Keppel E., Bowey J. E., Speck A. K., 2000b, in Salama A., Kessler M. F., Leech K., Schulz B., eds, *ESA-SP 456, ISO Beyond the Peaks: The 2nd ISO Workshop on Analytical Spectroscopy*. ESA Publications Division, Noordwijk, p. 343
- Hofmeister A. M., Keppel E., Speck A. K., 2003, *MNRAS*, 345, 16
- Hoppe P., Ott U., 1997, in Bernatowicz Th. J., Zinner E., eds, *AIP Conf. Ser. Vol. 402, Astrophysical Implications of the Laboratory Study of Presolar Materials*. Am. Inst. Phys., Woodbury, NY, p. 27
- Jones B., Merrill K. M., Puetter R. C., Willner S. P., 1978, *AJ*, 83, 1437
- Kemper F., Jäger C., Waters L. B. F. M., Henning Th., Molster F. J., Barlow M. J., Lim T., de Koter A., 2002, *Nat*, 415, 295
- Kemper F., Vriend W. J., Tielens A. G. G. M., 2004, *ApJ*, 609, 826
- Klanjšek Gunde M., Maček M., 2001, *Physica Status Solidi A*, 183, 2, 439
- Klein C., Hurlbut C. S., Jr, eds, 1993, *Manual of Mineralogy*, 21st edn. John Wiley & Sons, New York, p. 681
- Lambert D. L., Gustafsson B., Eriksson K., Hinkle K. H., 1986, *ApJS*, 62, 373
- Laurent Y., Lang J., Le Bihan M. T., 1968, *Acta Crystallogr. B*, 24, 494
- Lee M. R., Russell S. S., Arden J. W., Pillinger C. T., 1995, *Meteoritics*, 30, 387
- Leech K. et al., 2003, in Mueller T. G., Blommaert J. A. D. L., Garcia-Lario P., eds, *The ISO Handbook, Vol. V – SWS – The Short Wavelength Spectrometer, version 2.0.1 (June 2003)*. ESA Publications Division, Noordwijk
- Li A., 2003, *ApJ*, 599, L45
- Lide D. R., ed., 2005, *CRC Handbook of Chemistry and Physics 2005–2006*, 86th edn.
- Lin Y., Amari S., Pravdivtseva O., 2000, *Lunar Planet. Sci. Conf.*, 31, 1431
- Lodders K., Amari S., 2005, *Chemie de Erde*, 65, 93
- Lodders K., Fegley B., Jr., 1995, *Meteoritics*, 30, 661
- Lodders K., Fegley B., Jr., 1997, in Bernatowicz Th. J., Zinner E., eds, *AIP Conf. Ser. Vol. 402, Astrophysical Implications of the Laboratory Study of Presolar Materials*. Am. Inst. Phys., Woodbury, NY, p. 391
- Lodders K., Fegley B. Jr., 1999, in Le Bertre T., Lebre A., Waekens C., eds, *IAU Symp. 191, Asymptotic Giant Branch Stars*. Astron. Soc. Pac., San Francisco, p. 279
- MacKay D. D. S., Charnley S. B., 1999, *MNRAS*, 302, 793
- Molster F. J. et al., 2001, *A&A*, 372, 165
- National Bureau of Standards (US) Monogr. 25, 1975, 12, 5
- Nittler L. R. et al., 1995, *ApJ*, 453, L25
- Nyquist R. A., Kagel R. O., 1971, *Infrared Spectra of Inorganic Compounds (3800–45 cm⁻¹)*. Academic Press, New York, p. 495
- Ohnaka K., Tsuji T., Aoki W., 2000, *A&A*, 353, 528
- Rouleau F., Martin P. G., 1991, *ApJ*, 377, 526
- Schirmacher V., Woitke P., Sedlmayr E., 2003, *A&A*, 404, 267
- Sharp C. M., Wasserburg G. J., 1995, *Geochim. Cosmochim. Acta*, 59, 1633
- Sloan G. C., Price S. D., 1995, *ApJ*, 451, 758
- Sloan G. C., Devost D., Bernard-Salas J., Wood P. R., Houck J. R., 2006, *ApJ*, 638, 472
- Speck A. K., Hofmeister A. M., 2004, *ApJ*, 600, 986
- Speck A. K., Barlow M. J., Skinner C. J., 1997, *MNRAS*, 20, 431
- Speck A. K., Hofmeister A. M., Barlow M. J., 1999, *ApJ*, 513, L87
- Speck A. K., Hofmeister A. M., Barlow M. J., 2000, in Sitko M. L., Sprague A. L., Lynch D. K., eds, *ASP Conf. Ser. Vol. 196, Thermal Emission Spectroscopy and Analysis of Dust, Discs, and Regoliths*. Astron. Soc. Pac., San Francisco, p. 281
- Speck A. K., Thompson G. D., Hofmeister A. M., 2005, *ApJ*, 634, 426
- Stevens J. A., Gear W. K., 2000, *MNRAS*, 312, L5
- Stroud R. M., Bernatowicz T. J., 2005, *Lunar Planet. Sci. Conf. XXXVI*
- Treffers R., Cohen M., 1974, *ApJ*, 188, 545
- Turner B. E., 1992, *ApJ*, 388, L35
- Volk K., Kwok S., Langill P. P., 1992, *ApJ*, 391, 285
- Volk K., Xiong G., Kwok S., 2000, *ApJ*, 530, 408
- Whittet D. C. B., 1992, *Dust in the Galactic Environment*. IoP Publishing, Bristol, p. 295
- Wyckoff R. W. G., 1963, *Crystal Structures*. 2nd edn, Vol. 1. John Wiley & Sons, New York
- Yang P., Fun H.-K., Rahman I. A., Saleh M. I., 1995, *Ceram. Int.*, 21, 137
- Yin Z., Smith F. W., 1990, *Phys. Rev. B*, 42, 3666
- Zijlstra A. et al. 2006, *MNRAS*, 370, 1961

SUPPLEMENTARY MATERIAL

The following supplementary material is available for download as part of the full-text version of the article from <http://www.blackwell-synergy.com>. All of the supplementary merged spectra are limited to 1800 cm⁻¹.

Appendix. Supplementary symmetry analyses for nitride compounds, given in Schoenflies notation (to relate to space groups, see Fateley, Mc Devitt & Bentley 1971). Includes Tables A1–A4.

Table S1. A tab-delimited text file of the merged mid- and far-IR thin film absorbance spectra of spectrally subtracted α -Si₃N₄ (Fig. 1, upper panel).

Table S2. A tab-delimited text file of the calculated mass absorption coefficients for spectrally subtracted α -Si₃N₄ (Fig. 1, upper panel).

Table S3. A tab-delimited text file of the merged mid- and far-IR thin film absorbance spectra of spectrally subtracted β -Si₃N₄ (Fig. 1, lower panel).

Table S4. A tab-delimited text file of the calculated mass absorption coefficients for spectrally subtracted β -Si₃N₄ (Fig. 1, lower panel).

Table S5. A tab-delimited text file of the merged mid- and far-IR thin film absorbance spectra of AlN (Fig. 2, top panel).

Table S6. A tab-delimited text file of the calculated mass absorption coefficients for AlN (Fig. 2, top panel).

Table S7. A tab-delimited text file of the merged mid- and far-IR thin film absorbance spectra of Mg₃N₂ (Fig. 2, centre panel).

Table S8. A tab-delimited text file of the calculated mass absorption coefficients for Mg₃N₂ (Fig. 2, centre panel).

Table S9. A tab-delimited text file of the merged mid- and far-IR thin film absorbance spectra of Ca₃N₂ (Fig. 2, bottom panel).

Table S10. A tab-delimited text file of the calculated mass absorption coefficients for Ca₃N₂ (Fig. 2, bottom panel) using ρ_{calc} for orthorhombic Ca₃N₂ (Lide 2002). For the cubic case, κ_{abs} can be calculated using the value of Laurent et al. (1968) given in Table 1.

This paper has been typeset from a \TeX/L\TeX file prepared by the author.